



HAL
open science

Control of binary states of ferroic orders in bi-domain BiFeO₃ nanoislands

N. Alyabyeva, A. Ouvrard, M. Bavencoffe, I. Lindfors-Vrejoiu, A.
Kolomiytsev, M. Solodovnik, O. Ageev, D. Mcgrouter

► **To cite this version:**

N. Alyabyeva, A. Ouvrard, M. Bavencoffe, I. Lindfors-Vrejoiu, A. Kolomiytsev, et al.. Control of binary states of ferroic orders in bi-domain BiFeO₃ nanoislands. Applied Physics Letters, 2020, 116 (19), pp.192904. 10.1063/1.5143444 . hal-03087921

HAL Id: hal-03087921

<https://hal.science/hal-03087921>

Submitted on 24 Dec 2020

HAL is a multi-disciplinary open access archive for the deposit and dissemination of scientific research documents, whether they are published or not. The documents may come from teaching and research institutions in France or abroad, or from public or private research centers.

L'archive ouverte pluridisciplinaire **HAL**, est destinée au dépôt et à la diffusion de documents scientifiques de niveau recherche, publiés ou non, émanant des établissements d'enseignement et de recherche français ou étrangers, des laboratoires publics ou privés.

Control of Binary States of Ferroic Orders in Bi-domain BiFeO₃ Nanoislands

N. Alyabyeva^{1,2,3,a)}, A. Ouvrard³, M. Bavencoffe⁴, I. Lindfors-Vrejoiu⁵, A. Kolomyitsev², M. Solodovnik², O. Ageev² and D. McGrouther¹

¹School of Physics & Astronomy, University of Glasgow, Glasgow G12 8QQ, UK

²Southern Federal University, Research and Educational Centre “Nanotechnology”, 347928, 2, Shevchenko Str., Taganrog, Russia

³Université Paris-Saclay, CNRS, Institut des Sciences Moléculaires d'Orsay, 91405, Orsay, France

⁴GREMAN UMR-CNRS 7347, Université de Tours, INSA Centre Val de Loire, 41000 Blois, France

⁵II. Physikalisches Institut, Universität zu Köln, 05937 Köln, Germany

^{a)}Electronic mail: natalia.alabyeva@u-psud.fr

ABSTRACT

Selective control of the switching path in multiferroics such as BiFeO₃ (BFO) is one of the main challenge for the design of non-volatile memories based on magnetoelectric coupling. Here, we demonstrate an alternative way to control binary states of ferroic orders (ferroelectric or ferroelastic) using an array of BFO nanoislands exhibiting two ferroelectric domains. The study of electronic transport properties and domain orientations using atomic force microscopy (AFM) based techniques enabled us to determine electric and mechanical parameters at which ferroelectric and ferroelastic resistive switching can be observed. Ferroelastic switching was associated with a symmetry-breaking induced by electromechanical coupling between the AFM tip and the BFO thin film. It led to out-of-plane polarization pinning that allows performing only in-plane switching accompanied with nucleation and propagation of a conductive domain wall. Nanoislands exhibited binary states of high (OFF) and low resistance (ON) controlled by the tip contact force and the external electric field, without scaling effect (down to 50 nm). High performance characteristics with up to 10⁴ OFF/ON ratio, good endurance and retention characteristics were evidenced. Binary states of different ferroic orders with selective control of switching mechanisms by flexoelectric effect can find potential application in non-volatile memory with multilevel data storage capacity.

Keywords: BiFeO₃ thin films, ferroelectric domains, domain wall, binary states, ferroelectric switching, ferroelasticity, flexoelectricity, focused ion beam, piezoresponse force microscopy, conductive atomic force microscopy, finite element method.

BiFeO₃ (BFO) is the one of the most promising multiferroics in which magnetoelectric coupling could potentially be controlled, thanks to its high ferroelectric ($T_C = 1143$ K) and antiferromagnetic ($T_N = 643$ K) phase transition temperatures, its high spontaneous polarization ($\sim 100 \mu\text{C}/\text{cm}^2$)^{1,2} accompanied by ferroic order parameters (ferroelectric, antiferromagnetic and ferroelastic) coupled at room temperature (RT).²⁻⁴ At RT in the absence of external electric field, BFO has a spontaneous electrical ordering along the $[111]_{pc}$ direction of its pseudocubic perovskite structure. The appearance of ferroelectricity in BFO leads to the distortion of its crystalline structure symmetry from cubic to rhombohedral and, as a result, to the ferroelastic deformation of its lattice.^{2,5} In this case, the ferroelectric polarization in BFO can have eight possible orientations corresponding to positive or negative directions of the four cube diagonals. When an external electric field is applied, the ferroelectric polarization performs orientation transitions of 180° , 71° and 109° .¹⁻⁶ Ferroelectric switching is associated with a 180° polarization reversal and the BFO unit cell is preserved (no ferroelastic switching), while both 71° and 109° polarization reversals are concomitant with different ferroelastic states along different distortion axis.^{3,4} Antiferromagnetic order in BFO can also be modified by ferroelastic switching that changes its modulated spin structure, leading to the appearance of magnetoelectric properties.² Magnetoelectric coupling in BFO has stimulated a lot of studies to design switchable devices. It was shown that the control of ferroelastic switching in a multi-domain system was a significant challenge because elastic interactions can destabilize small switched volumes, resulting in a back-switching at zero electric field and subsequently undesired volatility of stored information.^{7,4} Stabilizing ferroelastic switching is possible by eliminating the stress-induced instability, responsible for back-switching, using isolated monodomain BFO nanoislands.^{4,8} However, forming a bi-domain nanoisland where a single domain wall can be nucleated, propagated or pinned may provide additional ways to control electronic states. Indeed, it was reported that domain walls can be much more conductive than domains themselves, so that they can act as a current leakage path^{9,10} or they can be pinned, resulting in an incomplete domain switching⁶ or they can move over several nm reconfiguring domain's orientation.¹¹

In this work, we demonstrate the control of electronic transport properties in BiFeO₃ nanoislands composed of two ferroelectric domains. By mean of conductive atomic force microscopy (C-AFM) and piezoresponse force microscopy (PFM), we have probed domain orientations and domain wall motion induced by external electric field and tip contact force. The interplay of these parameters and confinement effect enabled us to stabilize electronic states of both domains and maintain the absence/presence of domain walls. This leads to the formation of binary states in BFO nanoislands linked to different ferroic orders.

70 nm-thick BiFeO₃ epitaxial film was grown using pulsed laser deposition on SrRuO₃ (SRO) buffer layer on DyScO₃(110) (DSO). Details of BFO thin film deposition and its crystallinity investigation by XRD are given elsewhere.^{12,13} Preliminary non-destructive visualization of out-plane (OP) and in-plane (IP) ferroelectric domains in the BFO film was done using scanning electron microscopy (SEM) with back-scattered electron detection, to select areas for further nanoisland fabrication.¹⁴ The most reported way to prepare high density array of BFO nanoislands uses thin anodic aluminium oxide as a nano-

template to form islands down to 40 nm.^{8,15,16} Another route is to use focused ion beam (FIB) etching, where the size of nanoislands is limited by the ion beam energy.¹⁷ The minimal size of nanoisland can reach down to 10 nm at 5 keV and 0.4 nA ion beam.¹⁸⁻²⁰ In our case, nanoislands composed of two BFO domains were prepared in several steps summarized in supplementary material [SM-I]: (i) passivation of BFO film by aluminum (Al) layer, (ii) chemical vapor deposition using FIB for growth of tungsten (W) matrix as a mask, (iii) FIB etching of W/Al/BFO structure down to SRO bottom electrode and (iv) removal of the Al layer in ultrasonic bath.

Electronic transport properties of BFO nanoislands and the impact of domain orientation have been studied using C-AFM and PFM working under air condition (Solver Next, NT-MDT). For that, standard commercial cantilevers (CoCr tips) with normal spring constant 3 N/m were used. Contact resistance between top (tip) and bottom (SRO) electrodes was probed by ramping the DC voltage V_{DC} at ± 8 V (applied on the tip) for different tip contact forces (0.3, 1 and 1.5 μN corresponding to 3, 5 and 7 GPa). Several cycles of measurements were performed for each contact force. Nanoislands were also scanned successively by C-AFM mode under ± 8 V with different contact forces in order to “write” states. The modified states were readout using OP and IP PFM tuned as in Ref. 14,21-23.

BFO nanoislands with cross-section are presented in **Figure 1(a)**. Current-voltage (I - V) characteristic done after Al elimination [**Fig. 1(b)**], shows that the SRO conductivity has almost an ohmic resistance appropriate for the bottom electrode. OP and IP PFM images show that each nanoisland is composed of two upward polarized domains rotated by a 71° relative to each other [**Fig. 1(c)** bottom], which is in agreement with the preselection of the area by PFM and SEM before the fabrication of nanoislands [**Fig. 1(c)** top].^{14,21}

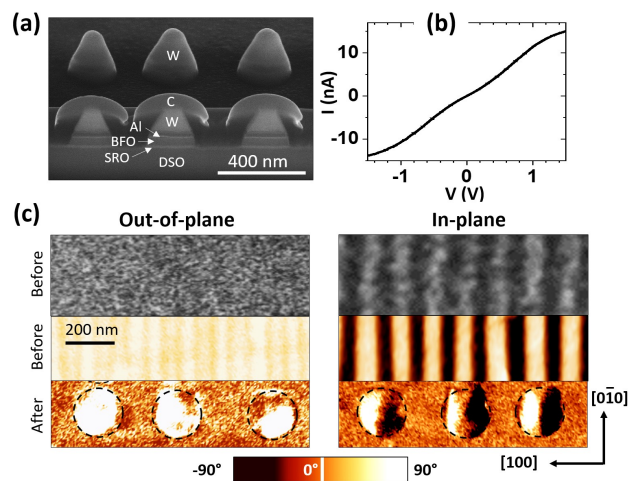


FIG. 1. (a) SEM images of BFO nanoislands with cross-section before Al removal; (b) I - V characteristics on SRO layer. (c) SEM (at different incidence angles relative to the surface normal: OP— 0° ; IP— 15°)¹⁴, OP and IP PFM images of BFO thin film before (top) and after (bottom) fabrication of nanoislands without Al layer.

The effect of the contact force on electronic transport properties in 200 nm large BFO nanoislands is shown in **Figure 2**. I - V measurements were carried out by ramping the bias voltage from 0 V to 8 V

or 10 V, back to 0 V and then reversing polarity to -8 V and returning to 0 V, repeatedly. For all tip forces, a large hysteresis of the I - V characteristic was clearly observed, but in a different manner. The initial current through the nanoisland with an up-polarization shows a diode-like behaviour with a resistance rapidly decreasing above 3 V when the tip forces are 0.3 μN [Fig. 2(a)] or 1 μN [Fig. 2(b)] and above 7 V at 1.5 μN [Fig. 2(c)]. By continuously ramping to positive voltage, the tip/BFO/SRO heterostructure changes from a high resistance state (OFF) to a low resistance state (ON). OFF/ON ratios at 0.3 or 1 μN are greater than 10, while at 1.5 μN it can reach up to $\sim 10^4$. Electronic structure transition from ON to OFF was also evidenced at negative voltages but only at low tip contact forces. At 1 μN , resistivity changes at -4 V with a very weak OFF/ON ratio while at 1.5 μN , the structure stays in OFF state. At any contact forces, the endurance measurements showed retention behaviour of switching, over more than 100 cycles without fatigue (loss of switchable polarization after cycles). All cycles for each force were averaged and the standard deviation is indicated by error bars. The impact of the contact force on polarization switching behaviour in bi-domain BFO nanoislands is evidenced by mean of OP and IP PFM (phase) measurements and shown in Figure 2. The deduced schematic representations of D_1 and D_2 domains polarization vectors are given and analysed in agreement with Ref. 14, 21. The initial state was probed at $V_{DC} = 0$ V and 0.3 μN contact force [Fig. 2(a)]. In correlation with Figure 1(c), both domains are upward polarized with 71° relative to each other in a non-neutral domain wall configuration (polarization vectors are head-to-head).³ After scanning nanoislands in C-AFM mode at 8 V and 0.3 μN , both domains underwent a 180° orientation transition from upward to downward and from right (left) to left (right) states for domain D_1 (D_2), in agreement with ferroelectric switching [Fig. 2(a)].^{4,8} Polarization back-switching⁶ was not observed, allowing to perform polarization reversal back to the initial state at -8 V. Subsequent orientation transitions at 8 V and 1 μN have exhibited a different behaviour for domain D_1 in comparison with lower contact force [Fig. 2(b)]. Both domain orientations have changed from upward to downward (OP), but IP component suggests that D_1 performed a 71° transition, on contrary to D_2 that switched by 180° . This domain configuration leads to the presence of a neutral domain wall. At -8 V, all domains have reversed their OP and IP states. Polarization vectors switched to upward and leftward states with a neutral domain wall. On contrary to 0.3 μN and 1 μN , OP orientations of both domains were not modified at 8 V and 1.5 μN [Fig. 2(c)]. At 8 V, domain orientations were kept upward, while in-plane component was changed for D_1 and D_2 with 71° , leading to the nucleation of non-neutral domain wall with 109° domain orientation relative to each other. Applying -8 V at high contact force brought domains back to their initial states, keeping the OP upward and changed the domain wall to a neutral state [Fig. 2(b)]. Interestingly, the domain wall width has increased from 10 nm at low force [Fig. 2(a)] to 40 nm at high force [Fig. 2(c)]. We hypothesize that the non-neutral domain configuration in a 3D confined structure under high tip contact force, forms inhomogeneous charge distribution along the domain wall, leading to its broadening that was visualized by PFM as a non-polar domain. Moreover, I - V characteristics probed on this domain wall show a relatively low resistance that can be considered as almost ohmic [SM-II]. BFO nanoislands confined down to 50 nm diameter were also studied [SM-III] and have evidenced a similar behaviour.

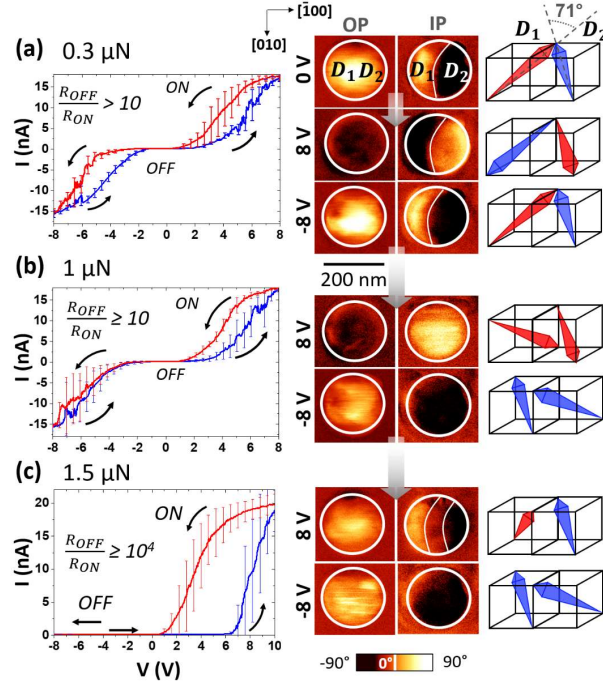


FIG. 2. Polarization dependent electronic transport characteristics of 200 nm large BFO nanoislands: I - V characteristics and OP and IP piezoresponse with suggested schematic illustration of both domains D_1 and D_2 , showing the polarization vector orientations with respect to the pseudocubic unit cell. Original domain state at 0 V and after polarization switching at 8 V and -8 V for (a) 0.3 μN , (b) 1 μN and (c) 1.5 μN tip contact forces. Grey arrows indicate the transition from a starting state to the next one.

A diode-like bipolar resistive switching was evidenced in BFO nanoislands at low (0.3 μN) tip contact force [Fig. 2(a)]. Hysteresis behaviour in I - V curves is a result of Schottky barrier modulation between top (tip) and bottom (SRO) electrodes, which depends on material work functions (ϕ). Band diagrams were described in Ref. 8, 24 for n-type BFO (2.8 eV band gap and 3.3 eV electron affinity). In the case of undoped BFO and CoCr tips ($\phi_{\text{tip}} > 4.8$ eV), the tip-BFO Schottky barrier is > 1.4 eV, while the SRO-BFO barrier ($\phi_{\text{SRO}} = 5.2$ eV) is > 1.9 eV, by assuming no BFO polarization. This state is called the virgin state (green dotted line in Figure 3). At low voltages, Schottky barriers are not modulated that prevents charge injection from the metal into the conduction band of BFO. Thus, the BFO nanoisland operates in a high-resistance state (HRS).^{8,24} When a high voltage is applied, polarization of BFO can be induced by diffusion of charged oxygen vacancies at interfaces and additional potential barriers appear as shown in Figure 3(a). Applying a depolarization voltage leads to a polarization switching. The BFO nanoisland operates in a low-resistance state (LRS) and switches back to HRS at high negative voltages. Between the metallic electrodes and BFO, depolarization voltage moves electrons that neutralize the positive boundary charges, while neutral oxygen vacancies (donor impurities) lose electrons and become positively charged to neutralize negative boundary charges.^{8,24,25} Polarization-modulated Schottky barriers are modified at both interfaces. Voltage thresholds (coercive voltages) in upward ($V_{th}^+ = 2.2$ V, $V_{th}^- = -1.8$ V) and downward ($V_{th}^+ = 1.1$ V, $V_{th}^- = -3.1$ V) states in Figure 2(a) can help determining

amplitudes of Schottky barriers $-eV_{th}^+ = -2.2$ eV, $-eV_{th}^- = +1.8$ eV in upward states and $-eV_{th}^+ = -1.1$ eV, $-eV_{th}^- = +3.1$ eV in downward states. The switchable diode behaviour in BFO is associated with a 180° orientation transition of the ferroelectric polarization according to the literature^{3-6,8,24} and is in a fairly good agreement with our PFM studies [Fig. 2(a)]. OP and IP PFM images show polarization switching at 8 V of both domains on 180° from their original state and vice-versa at -8 V.

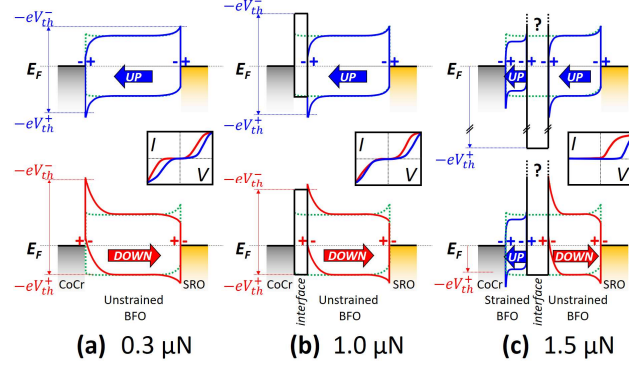


FIG. 3. Band diagrams of the tip/BFO/SRO heterostructure evidencing the intrinsic Schottky barriers at both interfaces for (a) 0.3 μ N, (b) 1 μ N and (c) 1.5 μ N tip forces for both polarization states (up and down). In insets are given sketches of I - V curves presented in Figure 2. $V_{th}^{+/-}$ are the voltage thresholds (coercive voltages) identified in Figure 2, at which the heterostructure becomes conductive. Green dotted lines correspond to the BFO virgin state.

I - V characteristics obtained on BFO nanoislands at 1 μ N tip force [Fig. 2(b)] show a similar behaviour than the previous case, associated to Schottky barrier modulation but with a larger (smaller) energy barrier of +0.6 eV (-0.5 eV) in upward (downward) state for negative voltages [Fig. 3(b)]. As a consequence, in contrary to lower contact force, HRS to LRS switching is only observed for positive voltage. For 1.5 μ N tip force a positive-forward rectifying resistive switching and 71° reversal of both D_1 and D_2 domains were found. Below 6 V and at negative voltages, nanoisland is always in HRS (OFF) and above 6 V, it switches to LRS (ON) [Fig. 2(c)]. The HRS at negative voltages can be explained by a strong increase of the tip-BFO Schottky barrier, similarly to the previous case at 1 μ N but with a larger magnitude. According to literature, applying a hydrostatic or an uniaxial strain on BFO for equivalent pressure range used here (1-10 GPa), lead to an overall decrease of its band gap, because of a better atomic orbital overlapping following the unit cell compression.^{26,27} It suggests that an increase of the band gap could not be considered in our case to explain the larger coercive voltages. However, the pressure is applied very locally at the tip apex that could strongly affect the electronic structure at the tip-surface interface and increase Schottky barriers. It was shown that in BFO layers thinner than 30-40 nm, the strain gradient created by the substrate misfit relaxation causes electromechanical coupling between electrical polarization and the strain gradient.²⁸ This flexoelectric effect can pin polarization in one state. Then, only positive-forward rectifying behaviour with HRS and LRS was observed in 30 nm thick BFO nanoislands.²⁹ Switching from HRS to LRS was explained by the transition from an insulating to a semiconducting state of the BFO/substrate interface, due to different oxygen vacancy densities that creates additional electrostatic potential barrier to electron migration.³⁰ In our case, applying a

sufficient uniaxial strain gradient with the AFM tip ($>1 \mu\text{N}$) at the surface of 70 nm thick BFO nanoislands creates flexoelectric effect explaining the positive-forward rectifying behaviour observed in **Figure 2(c)**.³¹ The disappearance of polarization switching at negative voltages could originate from the polarization pinning in the strained volume under the tip in upward state while deeper in the film the polarization can still be switched downward [**Fig. 3(c)**]. We suggest that at the interface between both strained and unstrained BFO appears a domain wall that can be switched from non-conducting (neutral) to conducting (non-neutral) state only at positive bias, in analogy with Ref. 29. At $1 \mu\text{N}$ where strain gradient is lower, a similar non-conducting interface is present at the surface [**Fig. 3(b)**]. Using higher tip load leads to a migration of this interface deeper in the film [**Fig. 3(c)**].

According to PFM, starting from a neutral domain wall at 8 V, domains do not perform any OP transitions, while IP states were modified, leading to a reversible polarization switching of 71° at -8 V of both domains [**Fig. 2(c)**]. This transition is accompanied with domain wall motion over ~ 40 nm. At this force, the positive threshold voltage is strongly affected from 6 to 1 V that indicates a change of the valence energy level. The absence of OP polarization switching may be related to a shrinkage of pseudocubic out-of-plane axis of BFO. This reduction of lattice degrees of freedom strongly affects the BFO electronic band structure [**Fig. 3(c)**] and can pin OP piezoresponse [**Fig. 2(c)**]. Finite element simulations [SM-IV] of tip/surface mechanical deformation have shown that a 3% of pseudocubic unit cell deformation under $1.5 \mu\text{N}$ along out-of-plane axis. These results are in agreement with recent studies that have evidenced the possibility to perform 71° switch and pin OP state in BFO thin film, by applying similar tip force.³¹ Similarly in our case, IP polarization switching of 71° for D_1 and D_2 is a result of symmetry breaking of the tip-surface interaction during domain state “writing”.^{32,14} Broken IP symmetry was persistent in our bi-domain configuration that allows performing stable 71° switching accompanied with nucleation, propagation and annihilation of conductive domain wall [**Fig. 2**]. Thereby, by modulating the tip contact force on the bi-domain nanoisland, it is possible to selectively pin or depin the OP piezoresponse and perform 71° ferroelastic or 180° ferroelectric switching, respectively suggesting potential application for multilevel data storage.

Different switching mechanisms related to either ferroelectric or ferroelastic order of BFO are observed in 200 nm large nanoislands exhibiting two ferroelectric domains, depending on the applied electric field and the tip contact force. We have shown that bipolar ferroelectric resistive switching (180° reversal), without fatigue or polarization pinning effects, can be observed above threshold voltages (± 8 V) for low contact forces ($<1 \mu\text{N}$). Increasing of the applied force to $1.5 \mu\text{N}$ leads to a pinning of the OP polarization vector due to a decrease of lattice degrees of freedom of the BFO unit cell, which strongly modifies the tip/BFO interface due to flexoelectric effect. Furthermore, this electromechanical coupling of polarization vector with the strain gradient in BFO allows a selective control of nucleation and motion of conductive domain wall. Ferroelectric and ferroelastic switching have large OFF/ON resistance ratios (from 10 to 10^4) and good endurance over 100 cycles. Decreasing lateral size of nanoislands did not significantly impact threshold voltages. Nanoislands as small as 50 nm still exhibited good endurance and retention characteristics for both ferroelectric and ferroelastic switching. The ability to perform selective control of polarization switching path using flexoelectric effect by

maintaining strain gradient at different electric fields in 3D confined BFO could bring ways to control ferroic orders necessary for magnetoelectric devices.

See in [supplementary materials](#): **(SM-I)** Fabrication of nanoislands; **(SM-II)** Conductivity of the domain wall in bi-domain BFO nanoislands; **(SM-III)** Lateral scaling of the nanoislands down to 50 nm; **(SM-IV)** COMSOL modelling of shrinkage of BFO pseudocubic unit cell.

This work was conducted in the frame of collaboration with Materials and Condensed Matter Physics Group, University of Glasgow, UK and Research and Educational Centre “Nanotechnology” of Southern Federal University, Russia.

References

- ¹P. Rovillain, R. de Sousa, Y. Gallais, A. Sacuto, M. A. Méasson, D. Colson, A. Forget, M. Bibes, A. Barthélémy, M. Cazayous, *Nat. Mater.* **9**, 975–979 (2010).
- ²T. Zhao, A. Scholl, F. Zavaliche, K. Lee, M. Barry, A. Doran, M. P. Cruz, Y. H. Chu, C. Ederer, N. A. Spaldin, R. R. Das, D. M. Kim, S. H. Baek, C. B. Eom, R. Ramesh, *Nat. Mater.* **5**, 823–829 (2006).
- ³S. H. Baek, C. B. Eom, *Phil. Trans. R. Soc. A* **370**, 4872–4889 (2012).
- ⁴S. H. Baek, H.W. Jang, C. M. Folkman, Y. L. Li, B. Winchester, J. X. Zhang, Q. He, Y. H. Chu, C. T. Nelson, M. S. Rzchowski, X. Q. Pan, R. Ramesh, L. Q. Chen, C. B. Eom, *Nat. Mater.* **9**, 309–314 (2010).
- ⁵J. B. Neaton, C. Ederer, U. V. Waghmare, N. A. Spaldin, K. M. Rabe, *Phys. Rev. B* **71**, 014113 (2005).
- ⁶S.-H. Baek, C. M. Folkman, J.-W. Park, S. Lee, C.-W. Bark, T. Tybell, C.-B. Eom, *Adv. Mater.* **23**, 1621–1625 (2011).
- ⁷M. P. Cruz, Y. H. Chu, J. X. Zhang, P. L. Yang, F. Zavaliche, Q. He, P. Shafer, L. Q. Chen, R. Ramesh, *Phys. Rev. Lett.* **99**, 217601 (2007).
- ⁸S. Hong, T. Choi, J. H. Jeon, Y. Kim, H. Lee, H.-Y. Joo, I. Hwang, J.-S. Kim, S.-O. Kang, S. V. Kalinin, B. H. Park, *Adv. Mater.* **25**, 2339–2343 (2013).
- ⁹J. Seidel, L. W. Martin, Q. He, Q. Zhan, Y.-H. Chu, A. Rother, M. E. Hawkrige, P. Maksymovych, P. Yu, M. Gajek, N. Balke, S. V. Kalinin, S. Gemming, F. Wang, G. Catalan, J. F. Scott, N. A. Spaldin, J. Orenstein, R. Ramesh, *Nat. Mater.* **8**, 229–234 (2009).
- ¹⁰S. Farokhipoor, B. Noheda, *Phys. Rev. Lett.* **107**, 127601 (2011).
- ¹¹P. Sharma, Q. Zhang, D. Sando, C. H. Lei, Y. Liu, J. Li, V. Nagarajan, J. Seidel, *Scientific Adv.* **3**, 1700512 (2017).
- ¹²F. Johann, A. Morelli, I. Vrejoiu, *Phys. Status Solidi B* **249**(11), 2278–2286 (2012).
- ¹³F. Johann, A. Morelli, D. Biggemann, M. Arredondo, I. Vrejoiu, *Phys. Rev. B* **84**, 094105 (2011).
- ¹⁴N. Alyabyeva, A. Ouvrard, I. Lindfors-Vrejoiu, O. Ageev, D. McGrouther, *Appl. Phys. Lett.* **111**, 222901 (2017).
- ¹⁵J. Wua, Z. Fan, D. Xiao, J. Zhu, J. Wang, *Prog. in Mater. Science* **84**, 335–402 (2016).
- ¹⁶S. Hyun, H. Seo, Il-K. Yang, Y. Kim, G. Jeon, B.-y. Lee, Y. H. Jeong, Y. Kim, J. K. Kim, *J. Mater. Chem. C* **3**, 2237 (2015).
- ¹⁷A. Morelli, F. Johann, N. Schammelt, D. McGrouther, I. Vrejoiu, *J. of Appl. Phys.* **113**, 154101 (2013).
- ¹⁸M. D. Henry, M. J. Shearn, B. Chhim, A. Scherer, *Nanotech.* **21**, 24, 245303 (2010).
- ¹⁹O. A. Ageev, B. G. Konoplev, *Nanotechnology in microelectronics*, Nauka, Russia, 511 (2019).
- ²⁰O. A. Ageev, A. V. Vnukova, A. L. Gromov, A. S. Kolomyitsev, B. G. Konoplev, S. A. Lisitsyn, A. M. Alekseev, *Nanotech. in Russia* **9**, 26–30 (2014).

- ²¹N. Alyabyeva, A. Ouvrard, I. L.-Vrejoiu, A. Kolomyitsev, M. Solodovnik, O. Ageev, D. McGrouther, *Phys. Rev. Mater.* **2**, 064402 (2018).
- ²²M. Bah, N. Alyabyeva, R. Retoux, F. Giovannelli, M. Zaghrioui, A. Ruyter, F. Delorme, I. M. Laffez, *RSC Adv.* **6**, 49060 (2016).
- ²³S. V. Kalinin, A. Gruverman, *Scanning probe microscopy of functional materials*, Springer Science & Business Media, Berlin, 2010.
- ²⁴C. Wang, K.-j. Jin, Z.-t. Xu, Le Wang, C. Ge, H.-b. Lu, H.-z. Guo, M. He, G.-z. Yang, *Appl. Phys. Lett.* **98**, 192901 (2011).
- ²⁵G. L. Yuan, J. Wang, *Appl. Phys. Lett.* **95**, 252904 (2009).
- ²⁶M. Guennou, P. Bouvier, G. S. Chen, B. Dkhil, R. Haumont, G. Garbarino, J. Kreisel, *Phys. Rev. B* **84**, 174107 (2011).
- ²⁷H. Dong, Z. Wu, S. Wang, W. Duan, J. Li, *Appl. Phys. Lett.* **102**, 072905 (2013).
- ²⁸Y. Li, C. Adamo, P. Chen, P. G. Evans, S. M. Nakhmanson, W. Parker, C. E. Rowland, R. D. Schaller, D. G. Schlom, D. A. Walko, H. Wen, Q. Zhang, *Scien. Rep.* **5**, 16650 (2015).
- ²⁹J. H. Jeon, H.-Y. Joo, Y.-M. Kim, D. H. Lee, J.-S. Kim, Y. S. Kim, T. Choi, B. H. Park, *Scien. Rep.* **6**, 23299 (2016).
- ³⁰D. Lee, S. H. Baek, T. H. Kim, J.-G. Yoon, C. M. Folkman, C. B. Eom, T. W. Noh, *Phys. Rev. B* **84**, 125305 (2011).
- ³¹S. M. Park, Bo Wang, S. Das, S. C. Chae, J.-S. Chung, J.-G. Yoon, L.-Q. Chen, S. Mo Yang, T. W. Noh, *Nat. Nanotech.* **13**, 366–370 (2018).
- ³²N. Balke, S. Choudhury, S. Jesse, M. Huijben, Y. H. Chu, A. P. Baddorf, L. Q. Chen, R. Ramesh, S. V. Kalinin, *Nat. Nanotech.* **4**, 868–875 (2009).

Supplementary materials

(SM-I) Fabrication of nanoislands

The fabrication of nanoislands composed of two domains based on BFO/SRO/DSO heterostructure was done in several steps in analogy with our previous work.¹ First, we used SEM with back-scattered electron detection, to perform preliminary non-destructive visualization of out-plane (OP) and in-plane (IP) ferroelectric domains in the BFO film to select areas for further nanoisland fabrication.² **Figure SM-1** summarizes all fabrication steps. First, BFO surface was passivated by 15 nm thick Al film [**Fig. SM-1(a)**], using magnetron sputtering (Emitech k575x, Quorum Technologies, UK). At the second step, the tungsten (W) islands, used as a mask, were deposited by chemical vapour deposition using FIB (Nova NanoLab 600, FEI, Netherlands) [**Fig. SM-1(b)**]. Then, the surface was etched down to the SRO layer, using FIB, in order to form well separated BFO nanoislands connected by the bottom SRO electrode [**Fig. SM-1(c)**]. Carbon (C) protection layer was deposited on the first array of nanoislands to perform cross-section imaging. The close-up of the nanostructure cross-section is shown in **Figure SM-2(b)** and schematically represented in **Figure SM-2(c)**. The electrical contact to the SRO layer was performed using FIB, by etching Al/BFO down to SRO and depositing C contact (not shown here). The ion beam parameters for W and C deposition and etching were 30 kV and 30 pA. Under these conditions, gallium ions can be embedded in each side of W/Al/BFO islands down to 20 nm depth that can alter BFO properties.^{3,4} Therefore, the minimal nanoisland size at these beam parameters is around 50 nm. At the final step, the Al layer has been removed by MF-CD26 chemical etching in an ultrasonic bath for 4 hours [**Fig. SM-1(d)**].

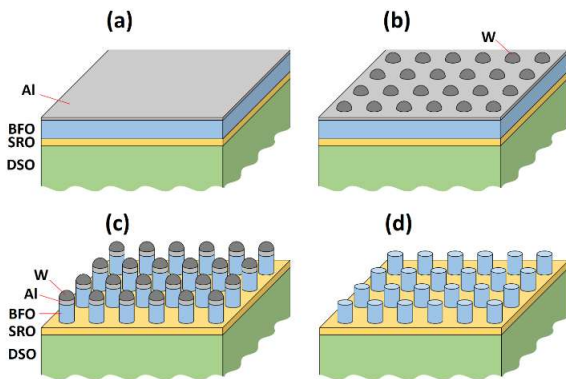


FIG. SM-1. Schematic representation of fabrication steps of the periodical array of BFO nanoislands on SRO/DSO: (a) Al deposition by magnetron sputtering; (b) growth of W mask by chemical vapor deposition using FIB; (c) FIB etching down to the bottom electrode; (d) chemical etching of the Al layer.

Three sets of BFO nanoislands prepared using different etching depths (~80 nm (I), 90 nm (II), 95 nm (III) deep) are presented in **Figure SM-2**. The close-up of nanoislands cross-section reveals that SRO electrode was affected by the etching in all areas, while in II and III the SRO thickness was significantly diminished [**Figure SM-2(b,c)**]. The profile and current-voltage (I - V) characteristics along the three etched areas done after Al elimination [**Fig. 3(a,b)**], show that SRO conductivities for 90 nm (II), 95 nm (III) deep zones are quite low (even by taking into account Ga⁺ doping of his areas) in comparison with 80 nm deep area (I) that has almost an ohmic resistance. Based on this, nanoislands of (I) area were selected for further studies.

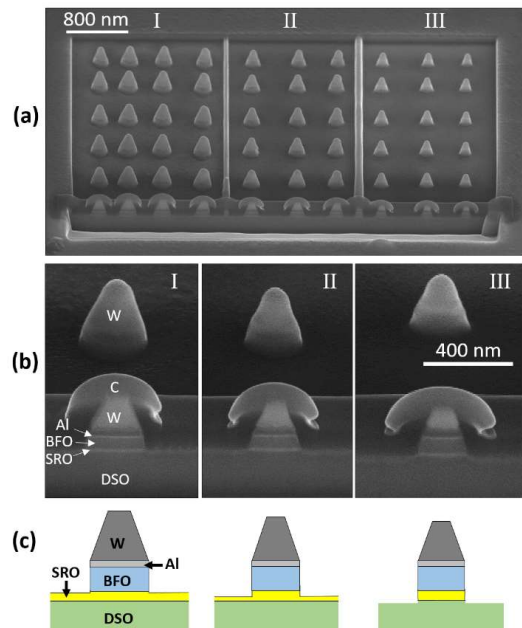


FIG. SM-2. SEM images of BFO nanoislands (side view) prepared with (I) 80 nm, (II) 90 nm, (III) 95 nm depth level before Al removal (a) and close-up of nanoislands cross-section in each area (b). (c) Schematic representation of cross-section without carbon-protection layer.

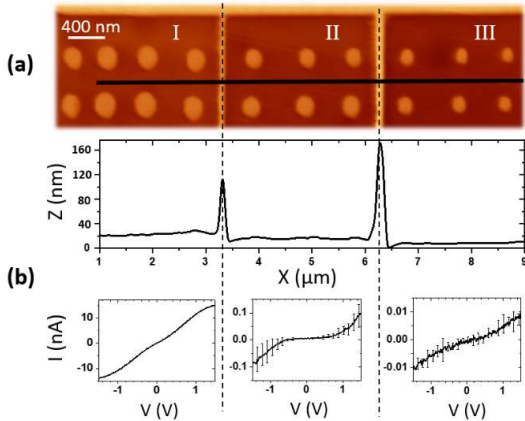


FIG. SM-3. BFO nanoislands after aluminum removal: (a) AFM images of the three areas with nanoislands, with a different thickness of the underlying SRO (as in Fig. SM-2); (b) profile along the black line in (a) and I - V characteristics on SRO of each area. (c) OP and IP PFM images of BFO thin film before (top) and after (bottom) fabrication of nanoislands.

(SM-II) Conductivity of the domain wall in bi-domain BFO nanoislands

A series of measurements along the domain wall of bi-domain nanoislands at a tip contact force of 1.5 μ N were performed, averaged over cycles and plotted in Figure SM-4(a,b). Error bars indicate the standard deviation. The conductive domain wall has a bipolar resistive switching behaviour: switching from diode-like OFF state to almost ohmic ON state. The threshold voltages are ± 5 V with weak OFF-ON ratio below 10. We suggest that such a hysteresis behaviour in domain wall is related to the formation of conducting filaments (leakage current paths) linked to electron conduction between the electrodes (tip and SRO), which induces migration of oxygen vacancies under electric field along the domain wall.

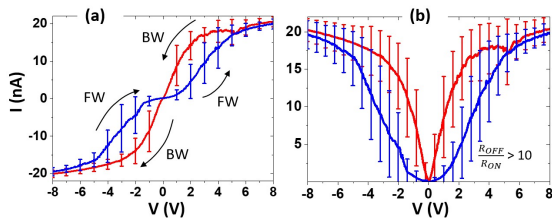


FIG. SM-4. Electronic transport characteristics of domain wall: (a-b) Averaged forward and backward I - V characteristics in linear and semi-logarithmic scales where error bars indicate standard deviations. FW: forward and BW: backward direction of switching pathway.

(SM-III) Lateral scaling of the nanoislands down to 50 nm

Lateral size effect on domain polarization switching was studied on 100 nm, 70 nm and 50 nm diameter BFO nanoislands [Fig. SM-5(a)] prepared all in the way sketched in Fig. SM-1. Nanoislands were composed of two domains with polarization vectors rotated by 71° relative to each other, in agreement with Refs. 2, 5 and Figures 1 and 2 (article). Hysteresis in I - V curves were observed for all nanoislands, where bipolar resistive switching was present at 0.3 μ N [Fig. SM-4(b)] and switching at 1.5 μ N tip forces for positive bias only [Fig. SM-4(c)]. For 100 nm nanoislands and 0.3 μ N, OFF/ON states were favoured at threshold voltages around 2 V and -4 V. For smaller nanoislands, threshold voltages were slightly higher, up to 5 V and -7 V. On contrary, the switching that appeared at 1.5 μ N, did not exhibit a size effect and the nanoisland charge state was modified at 8 V. For both tip forces, time dependent current measurements at different voltages are in agreement with I - V characteristics and evidence an excellent retention of low resistance (ON) and high resistance (OFF) states over several hours with a large OFF/ON ratio (more than 10 for ferroelectric and 10^4 for ferroelastic switching). Small current drop was observed at $t = 40$ min for 0.3 μ N that may originate from a change of the contact area at the tip/BFO interface due to feeble tip-surface interaction.⁶

(SM-IV) COMSOL modelling of shrinkage of BFO pseudocubic unit cell

The contact between the AFM tip and the BFO layer has been simulated thanks to COMSOL Multiphysics[®] FEA software, using the Acoustic Module and the MEMS Module, in order to investigate the spatial distribution of the lattice strain on the z-x plane of pseudocubic BFO unit cell. The calculation was performed for a system in which a CoCr AFM tip hemisphere with a radius of 45 nm is put in contact with a 70 nm thick and 200 nm radius BFO cylinder. Due to the geometry of the tip and to be closer to reality, a 2D axisymmetric model is realized with a triangular mesh made of 26013 elements. As the two objects touch each other, the constraints are enforced on the BFO destination surface. Then a form assembly is created and the contact region is meshed finer than elsewhere. The

mechanical effect of the BFO substrate layer is taken into account thanks to a fixed constraint mechanical condition on the lower border of the BFO layer. The fields of displacement and velocity for each point of the mesh are initially null. Then, a tip contact force is applied on the upper border of the hemisphere. The stationary contact problem was solved iteratively using the Newton-Raphson method. To get a better convergence, a continuation procedure is used: the applied force ramps from 0 to 1.5 μN using a logarithmic increment. Then, the resolution of the stationary problem makes it possible to obtain the displacement field, and then the c/a ratio, under AFM tip forces of 0.3 and 1.5 μN . Tip and BFO input parameters summarized in the Table 1.

Table S1. Tip and BFO input parameters

Parameters	Tip: CoCr alloy	Thin film: BFO
Tip radius/film thickness	45 nm	70 nm
Young's module	~ 230 GPa	~ 172 GPa
Poisson's ration	0.29	0.3
Density	8400 kg/m^3	8340 kg/m^3

Figure SM-6 evidences tip/surface mechanical deformation under 0.3 μN and 1.5 μN tip contact force. We deduce that a 3% difference in lattice parameter enables to pin OP polarization (shown by PFM) in upward direction at 1.5 μN .

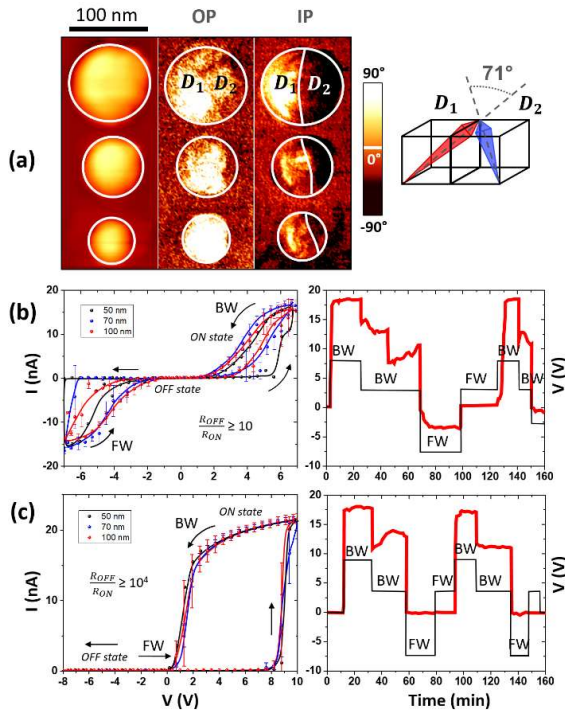


FIG. SM-5. Lateral size effect on electronic transport characteristics of BFO nanoislands. (a) Topography, OP and IP PFM images of 100 nm, 70 nm and 50 nm nanoislands. (b, c)-left: Averaged I - V characteristics over several cycles and their standard deviation is represented by error bars. (b, c)-right: Time-dependent measurements (current in red, voltage in black) at (b) 0.3 μN and (c) 1.5 μN tip contact forces, for forward (FW) and backward (BW) direction of the switching pathway.

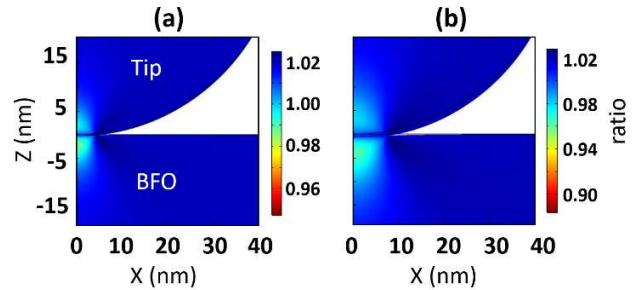


FIG. SM-6. (a,b) Simulated local distribution of out-of-plane/in-plane lattice deformation ratio in BFO thin film for 0.3 μN (a) and 1.5 μN (b) tip constant forces.

References

- ¹A. Morelli, F. Johann, N. Schammelt, D. McGrouther, I. Vrejoiu, J. of Appl. Phys. **113**, 154101 (2013).
- ²N. Alyabyeva, A. Ouvrard, I. Lindfors-Vrejoiu, O. Ageev, D. McGrouther, Appl. Phys. Lett. **111**, 222901 (2017).
- ³M. D. Henry, M. J. Shearn, B. Chhim, A. Scherer, Nanotech. **21**, 24, 245303 (2010).
- ⁴O. A. Ageev, B. G. Konoplev, Nanotechnology in microelectronics, Nauka, Russia, 511 (2019).
- ⁵N. Alyabyeva, A. Ouvrard, I. L.-Vrejoiu, A. Kolomiitsev, M. Solodovnik, O. Ageev, D. McGrouther, Phys. Rev. Mater. **2**, 064402 (2018).
- ⁶O. A. Ageev, N. I. Alyabieva, B. G. Konoplev, V. A. Smirnov, V. V. Tkachuk, Adv. Mater. Res. **894**, 374-378 (2014).